**REGULAR PAPER**

# On Accurate and Efficient Judgment Method of Milling Stability Based on Predictor–Corrector Scheme

Weida Lou[1] · Guohua Qin[1,2] · Xiaochun Lai[3] · Yuanjun Hou[2]

## Abstract

The accurate and efficient identification of milling stability region is key to suppressing chatter and improving production efficiency. Therefore, the theory of "predictor–corrector" is dependent on proposing a new method for milling stability prediction. Firstly, the delay differential equation on regenerative chatter is turned into the state space expression. Then, the Milne formula is used to predict the displacement whereas the Simpson formula corrects this predicted value. Furthermore, a discrete prediction-correction expansion with higher precision is constructed to obtain the state transition express. Based on the Floquet theory, the milling stability can be judged. Finally, the comparison of local discretization errors obtained by the proposed method with other methods shows that the proposed method has a faster convergence speed than the contrast methods. Obviously, under the same discretization conditions, the proposed method can not only achieve higher computational accuracy than the contrast methods but also obtain faster computational efficiency. Both 29 groups of the simulation results and 9 groups of experimental measurements can further validate the presented method in actual prediction effect.

**Keywords** Milling process · Stability lobe diagram · Linear multi-step methods · Milne–Simpson · Semi-discretization method

## 1 Introduction

Milling technology plays an important role in aerospace and mechanical engineering. In comparison to traditional material removal methods, it can maintain relatively lower cutting forces and faster material removal rates so that it can achieve better part surface quality. However, milling chatter is an important problem that seriously affects the workpiece surface quality and production efficiency. One of the most important factors that cause milling chatter is the regeneration effect [1]. The regenerative chatter results mainly from the phase difference caused by the inconsistent cutting thickness of two adjacent tooth passing periods.

✉ Guohua Qin
  qghwzx@126.com

1  School of Mechanical Engineering, Northwestern Polytechnical University, Xi'an 710072, China

2  School of Aeronautical Manufacturing Engineering, Nanchang Hangkong University, Nanchang 330063, China

3  Jiangxi Education International Cooperation and Teacher Development Center, Jiangxi Provincial Department of Education, Nanchang 330038, China

In the field of mechanical manufacturing, the prediction of milling chatter has always attracted lots of attention [1, 2, 5]. In recent decades, extensive and profound theoretical research and experimental verification have been carried out on regenerative chatter in academic and industrial circles [3–8]. Altintas et al. [9] used the Fourier expansion to propose a zero-order approximation (ZOA) method by preserving the zero-order term in the frequency domain. But ZOA is not suitable for the small radial depth of cut conditions. Merdol and Altintas [10] took into account the higher-order terms of the Fourier series to construct a multi-frequency (MF) solution for milling stable regions. Since MF must repeatedly search the chatter frequency, it is not computationally efficient. Bayly et al. [11] proposed a time finite element analysis (TFEA) method by using the weighted residual method to deduce the state transition matrix for the discretized cutting time nodes. Certainly, this method is not computationally efficient not to fully apply to all working conditions. Insperger et al. [12, 13] explored the semi-discretization method (SDM). The tooth passing period was discretized uniformly into small time intervals. The delay- and periodic-term of DDE took the averaged values of two endpoints in every time interval so that the DDE

could be transformed into an ordinary differential equation (ODE). Afterward, they again proposed a high-order SDM with higher algebraic accuracy [14]. Ding et al. [15] introduced the full-discretization method (FDM) based on the direct integration scheme. Also, Ding et al. [16] improved the FDM to obtain the second-order FDM by increasing the interpolation order on the state term. Though the 2nd FDM could improve the computational accuracy, the computational efficiency was decreased with the improvement of the interpolation order. Likewise, the state term of DDE can be interpolated by a third-order method [17, 18] and other FDM-based enhanced methods [19–23]. Niu et al. [24] proposed the generalized Runge–Kutta method (GRKM). Li et al. [25] proposed a complete discretization scheme (CDS). Zhang et al. [26] used Simpson numerical integration formula to propose a concise SLD method. By replacing the fourth-order Runge Kutta formula with the Euler formula in the CDS, Li et al. [27] obtained an improved Runge–Kutta method.

Accurate calibration of cutting force coefficients and accurate identification of tool system dynamic parameters are crucial for predicting milling stability correctly. Mostaghimi et al. [28] combined the artificial neural network and receptance coupling method to propose a method for predicting the dynamic parameters of the tool system. Kang et al. [29] used an optimization method to obtain coefficients from individual cutting conditions to identify cutting force coefficients. By modifying the design parameters to reduce the difference between the measured and simulated cutting forces, and to determine the optimal cutting force coefficient. Compared with traditional methods, the proposed method can predict the cutting force more accurately. In terms of SLD predictions, recently, Qin et al. [30] adopted the second-order Lagrange interpolation polynomial for the approximation of the displacement at every time node to propose a holistic-discretization method (HIM). Dai et al. [31] presented a precise integration method (PIM). Lou et al. [32] suggested a new numerical integration method by combining Lagrange interpolation with Cotes integral formula. Wu et al. [33] employed Milne and Simpson formula to obtain a correction method based on local truncation error being estimated in the state term. Moreover, they also proposed an implicit exponential fitting method based on the Fibonacci search [34]. Liu et al. [35] proposed an improved SDM based on predictor–corrector scheme. Qin et al. [36] used the Adams formula as a predictor item and proposed a series of predictor–corrector methods, which achieved good prediction results. Wei et al. [37] systematically analyzed the influence mechanism of parameters such as spindle speed and radial depth of cut on milling stability and established a three-dimensional stability prediction model under multiple milling parameters. Chen et al. [38] proposed a generalized numerical differentiation method for predicting the stability

of nonautonomous DDEs with periodic coefficients and discrete delays, and the theory was applied to predict the milling stability under multiple time delays.

As above stated, the general analyzing process of milling stability can be summarized as follows: By discretizing the tooth passing period of DDE, the numerical calculation method is adopted to deduce the state transition matrix. And then, the Floquet theory is depended on to carry out the chatter analysis. In fact, the aim of chatter analysis method is the realization of two seemingly contradictory aspects. One is to obtain a better calculation accuracy of the SLD under the small periodic discrete number. Another is to improve the computational efficiency as high as possible under the increase of periodic discrete numbers. However, today's prediction methods for SLD do not perfectly solve these two computation performance problems. Usually, the ODE can numerically be solved by a linear multi-step method. In the predictor–corrector linear multi-step method, the predictor value is calculated by using the explicit formula whereas the corrector value is calculated by using the implicit formula. It can always obtain better numerical stability for both low-order and high-order methods [39]. In this paper, Taylor expansion is used to obtain the higher-order Milne explicit formula and Simpson implicit formula so that a new Milne Simpson predictor–corrector method (MS-PCM) is applied to predict the milling stability region. It is worth mentioning that MS-PCM only needs to calculate three discrete point values for the next discrete point value whereas the same-order Adams [36] needs four discrete point values. Therefore, MS-PCM is of more simple calculation. Moreover, the Milne formula has the main truncation error coefficient of 14/45 while the Adams formula is 251/720. Obviously, the MS-PCM is slightly smaller mathematical calculation error than the Adams method [36].

The remainder of this paper is arranged as follows: Sect. 2 is to establish the dynamic model of two degrees of freedom (DOF) milling system. Section 3 is to give the detailed mathematical derivation of the MS-PCM. Section 4 illustrates the advantages of the MS-PCM over other methods. Section 5 demonstrates the accuracy and effectiveness of MS-PCM through numerical simulations and experiments. Finally, Sect. 6 is to summarize the characteristic conclusions of the MS-PCM.

## 2 Dynamics Model of Milling System

Without losing generality, suppose the workpiece is rigid but milling tool is flexible. Figure 1 is the two-DOF milling dynamic model along the feed direction $X$ and the workpiece wall thickness direction $Y$. The dynamic milling process with the regeneration effect [3, 4, 40] is written as
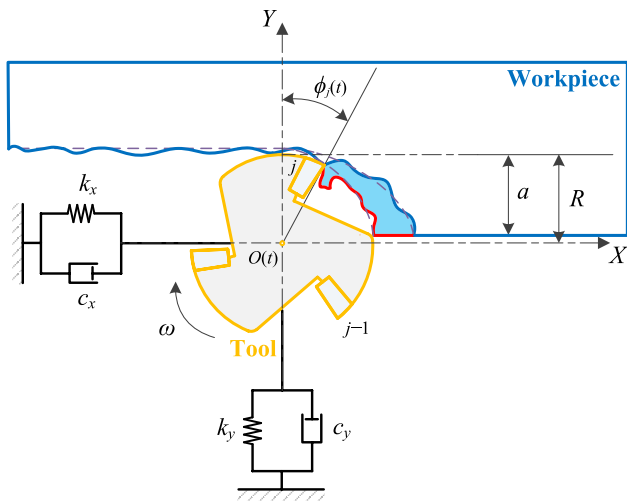
**Fig. 1** Two-DOF milling dynamics model

$$\mathbf{M}\ddot{\mathbf{q}}(t) + \mathbf{C}\dot{\mathbf{q}}(t) + \mathbf{K}\mathbf{q}(t) = \mathbf{Q}(t)[\mathbf{q}(t) - \mathbf{q}(t-\tau)] \tag{1}$$

where $\mathbf{M}$, $\mathbf{C}$ and $\mathbf{K}$ are the modal parameter matrices. $\mathbf{q}(t)$ is the vibration displacement vector of milling tool. $\tau = 60/N/\Omega$ is the time delay. $N$ is the tooth number. $\Omega$ is the spindle speed. $\mathbf{Q}(t) = \mathbf{Q}(t+\tau)$ is the dynamic milling force coefficient matrix whose expression is

$$\mathbf{Q}(t) = \begin{bmatrix} -a_p h_{xx}(t) & -a_p h_{xy}(t) \\ -a_p h_{yx}(t) & -a_p h_{yy}(t) \end{bmatrix} \tag{2}$$

where

$$\begin{cases} h_{xx}(t) = \sum_{j=1}^{N} g(\phi_j(t)) \sin(\phi_j(t))\left[K_t \cos(\phi_j(t)) + K_r \sin(\phi_j(t))\right] \\ h_{xy}(t) = \sum_{j=1}^{N} g(\phi_j(t))\cos(\phi_j(t))\left[K_t \cos(\phi_j(t)) + K_r \sin(\phi_j(t))\right] \\ h_{yx}(t) = \sum_{j=1}^{N} g(\phi_j(t)) \sin(\phi_j(t))\left[K_r \cos(\phi_j(t)) - K_t \sin(\phi_j(t))\right] \\ h_{yy}(t) = \sum_{j=1}^{N} g(\phi_j(t)) \cos(\phi_j(t))\left[K_r \cos(\phi_j(t)) - K_t \sin(\phi_j(t))\right] \end{cases} \tag{3}$$

where $h_{xx}(t)$, $h_{xy}(t)$, $h_{yx}(t)$, $h_{yy}(t)$ is milling force coefficient matrix. $K_t$ and $K_r$ are respectively milling force coefficients in the tangential and the normal direction. $\phi_j(t)$ is the current angular of the tooth $j$ which is expressed as

$$\phi_j(t) = \frac{2\pi\Omega}{60}t + \frac{2\pi(j-1)}{N} \tag{4}$$

$g(\phi_j(t))$ is a window function to judge whether the tooth $j$ is cutting and

$$g(\phi_j(t)) = \begin{cases} 1, & \phi_{st} < \phi_j(t) < \phi_{ex} \\ 0, & \text{other} \end{cases} \tag{5}$$

with the start angle $\phi_{st}$ of the $j$th tooth and exit angle $\phi_{ex}$. It is worth noting that there are $\phi_{st} = \arccos(2a/D - 1)$, $\phi_{ex} = \pi$ and $\phi_{st} = 0$, $\phi_{ex} = \arccos(1 - 2a/D)$ in the down milling and the up milling, respectively. $a$ is the radial depth of cut, $D$ is the diameter of the tool and $a/D$ is defined as the radial immersion ratio.

Let $\mathbf{p}(t) = \mathbf{M}\dot{\mathbf{q}}(t) + \mathbf{C}\mathbf{q}(t)/2$ and $\mathbf{V}(t) = [\mathbf{q}(t)\,\mathbf{p}(t)]^T$, Eq. (1) can be further expressed as

$$\dot{\mathbf{V}}(t) = \mathbf{L}\mathbf{V}(t) + \mathbf{\Theta}(t)[\mathbf{V}(t) - \mathbf{V}(t-\tau)] \tag{6}$$

with $\mathbf{L} = \begin{bmatrix} -\mathbf{M}^{-1}\mathbf{C}/2 & \mathbf{M}^{-1} \\ \mathbf{C}\mathbf{M}^{-1}\mathbf{C}/4 - \mathbf{K} & -\mathbf{C}\mathbf{M}^{-1}/2 \end{bmatrix}$, $\mathbf{\Theta}(t) = \begin{bmatrix} \mathbf{0} & \mathbf{0} \\ \mathbf{Q}(t) & \mathbf{0} \end{bmatrix}$.

Clearly, $\mathbf{L}$ is a constant coefficient matrix with only respect to the modal parameters. $\mathbf{\Theta}(t)$ is the periodic coefficient matrix which is related to the milling force coefficient. Just like the milling force coefficient matrix $\mathbf{Q}(t)$, $\mathbf{\Theta}(t)$ is also a periodic function of $\tau$, i.e., $\mathbf{\Theta}(t) = \mathbf{\Theta}(t+\tau)$.

## 3 MS-PCM Based Stability Analysis

Evidently, it is difficult in obtaining a strict analytical solution of Eq. (6). Therefore, a numerical method must be sophisticatedly adopted to solve Eq. (6).

Here, $t_0$ and $t_1$ are used to denote the initial time of a cutting period and the cut-in time of the cutter tooth, respectively. Moreover, the time $\tau + t_0$ is called the cut-out time of the cutter tooth. Thus, the time between $t_0$ and $t_1$ is named the free vibration period $t_f = t_1 - t_0$. Likewise, the time from $t_1$ to $\tau + t_0$ is defined as the forced vibration period. If $\tau - t_f$ is uniformly discretized into $m$ small intervals, the length of each interval is equal to $h = (\tau - t_f)/m$, as shown in Fig. 2. Thus, an arbitrary discrete time note point can be expressed as

$$t_i = t_0 + t_f + (i-1)h, \quad i = 1, 2, \ldots, m, m+1 \tag{7}$$

Similar to Volterra integral equations of the second kind [Refer to appendix 1], Eq. (6) can be expressed as the following form by considering $\mathbf{\Theta}(t)[\mathbf{V}(t) - \mathbf{V}(t-\tau)]$ as the inhomogeneous term of the homogeneous equation $\dot{\mathbf{V}}(t) = \mathbf{L}\mathbf{V}(t)$, i.e.,

$$\mathbf{V}(t) = e^{(t-t_0)\mathbf{L}}\mathbf{V}(t_0) + \int_{t_0}^{t} \left\{e^{(t-\sigma)\mathbf{L}}\mathbf{\Theta}(\sigma)[\mathbf{U}(\sigma) - \mathbf{U}(\sigma - \tau)]\right\}d\sigma \tag{8}$$

**Fig. 2** Schematic diagram of discrete tooth passing period
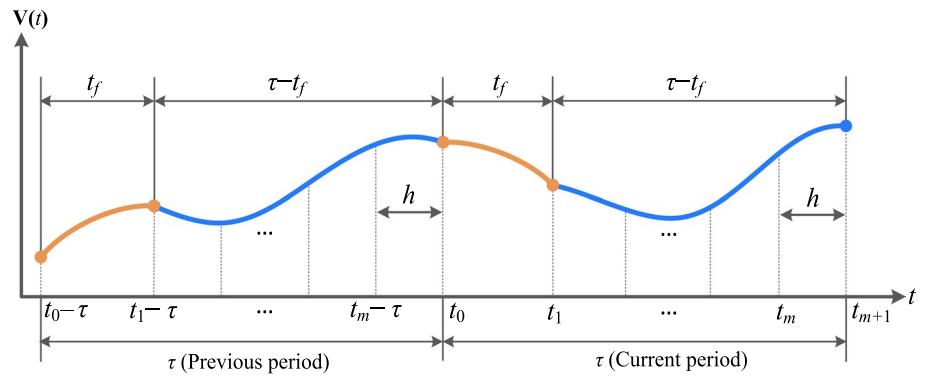


According to Eq. (7), if $t$ is within the $t_i$ and $t_{i+1}$, the following expression can be achieved as

$$\mathbf{V}(t) = \mathbf{s}(t, t_i) + \int_{t_i}^{t} \mathbf{R}[t, \sigma, \mathbf{V}(\sigma)] d\sigma \tag{9}$$

where $\mathbf{s}(t, t_i) = e^{(t-t_i)\mathbf{L}}\mathbf{V}(t_i)$, $\mathbf{R}[t, \sigma, \mathbf{V}(\sigma)] = e^{(t-\sigma)\mathbf{L}}\mathbf{\Theta}(\sigma)[\mathbf{V}(\sigma) - \mathbf{V}(\sigma - \tau)]$.

If the tooth is in the free vibration period $t_f$, the milling force coefficient matrix $\mathbf{Q}(t)$ is a zero matrix. Therefore, there is $\mathbf{\Theta}(\sigma) = \mathbf{0}$ in Eq. (8) so it is easy to obtain

$$\mathbf{V}(t) = \mathbf{s}(t, t_0) = e^{(t-t_0)\mathbf{L}}\mathbf{V}(t_0) \tag{10}$$

In the forced vibration period $\tau - t_f$, Eq. (8) is numerically integrated to achieve $\mathbf{V}(t)$ obviously. Consequently, the fourth-order Milne–Simpson predictor–corrector formula [Refer to appendix 2] is adopted to solve the $\mathbf{V}(t)$ at each discrete time note point when $t$ is not less than $t_4$. Thus, the linear multi-step formula of Eq. (8) can be described as

$$\mathbf{V}_{i+4}^{P} = \mathbf{s}(t_{i+4}, t_i) + \frac{4h}{3}\left[\begin{array}{l}2\mathbf{R}(t_{i+4}, t_{i+3}, \mathbf{V}_{i+3}) - \mathbf{R}(t_{i+4}, t_{i+2}, \mathbf{V}_{i+2}) \\ +2\mathbf{R}(t_{i+4}, t_{i+1}, \mathbf{V}_{i+1})\end{array}\right] \tag{11}$$

$$\mathbf{V}_{i+4}^{C} = \mathbf{s}(t_{i+4}, t_{i+2}) + \frac{h}{3}\left[\begin{array}{l}\mathbf{R}(t_{i+4}, t_{i+4}, \mathbf{V}_{i+4}^{P}) + 4\mathbf{R}(t_{i+4}, t_{i+3}, \mathbf{V}_{i+3}) \\ +\mathbf{R}(t_{i+4}, t_{i+2}, \mathbf{V}_{i+2})\end{array}\right] \tag{12}$$

Equations (11, 12) are both fourth-order algebraic precision formulas, called the Milne formula and Simpson formula, respectively. Their local truncation errors are $LTE_M = 14/45h^5\mathbf{V}^{(5)}(t) + O(h^6)$ and $LTE_S = -1/90h^5\mathbf{V}^{(5)}(t) + O(h^6)$, respectively. Obviously, Eq. (9) can be iteratively solved by taking Eq. (11) as the predictor item whereas Eq. (12) is the corrector item.

In the closed interval $[t_{i+4}, t_{m+1}]$, Eq. (9) can be further expressed as

$$\mathbf{V}_{i+4}^{P} = e^{4h\mathbf{L}}\mathbf{V}_i + \frac{4h}{3}\left[\begin{array}{l}2e^{h\mathbf{L}}\mathbf{\Theta}_{i+3}(\mathbf{V}_{i+3} - \mathbf{V}_{i+3-\tau}) - e^{2h\mathbf{L}}\mathbf{\Theta}_{i+2}(\mathbf{V}_{i+2} - \mathbf{V}_{i+2-\tau}) \\ + 2e^{3h\mathbf{L}}\mathbf{\Theta}_{i+1}(\mathbf{V}_{i+1} - \mathbf{V}_{i+1-\tau})\end{array}\right] \tag{13}$$

$$\mathbf{V}_{i+4}^{C} = e^{2h\mathbf{L}}\mathbf{V}_{i+2} + \frac{h}{3}\left[\begin{array}{l}\mathbf{\Theta}_{i+4}(\mathbf{V}_{i+4}^{P} - \mathbf{V}_{i+4-\tau}) + 4e^{h\mathbf{L}}\mathbf{\Theta}_{i+3}(\mathbf{V}_{i+3} - \mathbf{V}_{i+3-\tau}) \\ + e^{2h\mathbf{L}}\mathbf{\Theta}_{i+2}(\mathbf{V}_{i+2} - \mathbf{V}_{i+2-\tau})\end{array}\right] \tag{14}$$

For the sake of simplicity, $\mathbf{V}_i$, $\mathbf{V}_{i-\tau}$ and $\mathbf{\Theta}_{i-\tau}$ are used to denote $\mathbf{V}(t_i)$, $\mathbf{V}(t_i - \tau)$ and $\mathbf{\Theta}(t_i - \tau)$, respectively. Thus, the predictor–corrector linear multi-step formula of Eq. (9) can be obtained as

$$\mathbf{V}_{i+4} = e^{2h\mathbf{L}}\mathbf{V}_{i+2} + \left[\begin{array}{l}\frac{1}{3}he^{4h\mathbf{L}}\mathbf{\Theta}_{i+4}\mathbf{V}_i - \frac{1}{3}h\mathbf{\Theta}_{i+4}\mathbf{V}_{i+4-\tau} + \mathbf{G}_{i+1}(\mathbf{V}_{i+1} - \mathbf{V}_{i+1-\tau}) \\ + \mathbf{G}_{i+2}(\mathbf{V}_{i+2} - \mathbf{V}_{i+2-\tau}) + \mathbf{G}_{i+3}(\mathbf{V}_{i+3} - \mathbf{V}_{i+3-\tau})\end{array}\right] \tag{15}$$

with the expressions of $\mathbf{G}_{i+1}$, $\mathbf{G}_{i+2}$, $\mathbf{G}_{i+3}$ can be found in Appendix 3, similarly hereinafter.

By separating the time-delay term from the state term, Eq. (15) can be rewritten as

$$\mathbf{F}_{i+4-\tau}\mathbf{V}_{i+4-\tau} + \mathbf{F}_{i+3-\tau}\mathbf{V}_{i+3-\tau} + \mathbf{F}_{i+2-\tau}\mathbf{V}_{i+2-\tau} + \mathbf{F}_{i+1-\tau}\mathbf{V}_{i+1-\tau}$$
$$= \mathbf{F}_{i+4}\mathbf{V}_{i+4} + \mathbf{F}_{i+3}\mathbf{V}_{i+3} + \mathbf{F}_{i+2}\mathbf{V}_{i+2} + \mathbf{F}_{i+1}\mathbf{V}_{i+1} + \mathbf{F}_{i}\mathbf{V}_{i} \quad (16)$$

In fact, only when multiple initial values $\mathbf{V}(t_i)$, $\mathbf{V}(t_{i+1})$, $\mathbf{V}(t_{i+2})$ and $\mathbf{V}(t_{i+3})$ are determined in advance can Eq. (16) be taken effect for $\mathbf{V}(t_{i+4})$. In other words, if the MS-PCM is used to solve $\mathbf{V}(t_{i+4})$, the periodic discrete number $m$ must be satisfied the condition of $m \geq 4$. If $m < 4$, other methods such as the Newton–Cotes numerical integration can be used to solve $\mathbf{V}(t_i)$. At $t_1 = t_0 + t_f$, the relationship between the first value $\mathbf{V}_1$ of the state item and the last value $\mathbf{V}_{m+1-\tau}$ of the time-delay item can be easily obtained as

$$\mathbf{V}_1 = \mathbf{V}(t + t_f) = e^{t_f \mathbf{L}}\mathbf{V}_0 = e^{t_f \mathbf{L}}\mathbf{V}_{m+1-\tau} \quad (17)$$

In the case of $m = 1$, $\mathbf{V}_2$ can be implicitly expressed by the Trapezoidal formula as

$$\mathbf{V}_2 = e^{h\mathbf{L}}\mathbf{V}_1 + \frac{h}{2}\left[e^{h\mathbf{L}}\mathbf{\Theta}_1(\mathbf{V}_1 - \mathbf{V}_{1-\tau}) + \mathbf{\Theta}_2(\mathbf{V}_2 - \mathbf{V}_{2-\tau})\right] \quad (18)$$

By analogy, the time-delay term of Eq. (18) is separated from the state term to be achieved as

$$\mathbf{P}_{2,2-\tau}\mathbf{U}_{2-\tau} + \mathbf{P}_{2,1-\tau}\mathbf{U}_{1-\tau} = \mathbf{P}_{2,2}\mathbf{U}_2 + \mathbf{P}_{2,1}\mathbf{U}_1 \quad (19)$$

When $m = 2$, the Simpson method can be adopted to implicitly express $\mathbf{V}_3$ as

$$\mathbf{V}_3 = e^{2h\mathbf{L}}\mathbf{V}_1 + \frac{h}{3}\left[e^{2h\mathbf{L}}\mathbf{\Theta}_1(\mathbf{V}_1 - \mathbf{V}_{1-\tau}) + 4e^{h\mathbf{L}}\mathbf{\Theta}_2(\mathbf{V}_2 - \mathbf{V}_{2-\tau})\right.$$
$$\left. + \mathbf{\Theta}_3(\mathbf{V}_3 - \mathbf{V}_{3-\tau})\right] \quad (20)$$

Thus, the separation of the time-delay term with the state term can re-express Eq. (20) as

$$\mathbf{P}_{3,3-\tau}\mathbf{V}_{3-\tau} + \mathbf{P}_{3,2-\tau}\mathbf{V}_{2-\tau} + \mathbf{P}_{3,1-\tau}\mathbf{V}_{1-\tau} = \mathbf{P}_{3,3}\mathbf{V}_3 + \mathbf{P}_{3,2}\mathbf{V}_2 + \mathbf{P}_{3,1}\mathbf{V}_1 \quad (21)$$

But if $m = 3$, the Newton integral formula is selected to obtain $\mathbf{V}_4$ as

$$\mathbf{P}_{4,4-\tau}\mathbf{V}_{4-\tau} + \mathbf{P}_{4,3-\tau}\mathbf{V}_{3-\tau} + \mathbf{P}_{4,2-\tau}\mathbf{V}_{2-\tau} + \mathbf{P}_{4,1-\tau}\mathbf{V}_{1-\tau}$$
$$= \mathbf{P}_{4,4}\mathbf{V}_4 + \mathbf{P}_{4,3}\mathbf{V}_3 + \mathbf{P}_{4,2}\mathbf{V}_2 + \mathbf{P}_{4,1}\mathbf{V}_1 \quad (22)$$

By uniting Eqs. (16, 17, 19, 21) with Eq. (22), the discrete mapping relationship from the time-delay term to the state term can be constructed as

$$\mathbf{\Gamma}\begin{bmatrix} \mathbf{V}_1 \\ \mathbf{V}_2 \\ \vdots \\ \mathbf{V}_m \\ \mathbf{V}_{m+1} \end{bmatrix} = \mathbf{\Lambda}\begin{bmatrix} \mathbf{V}_{1-\tau} \\ \mathbf{V}_{2-\tau} \\ \vdots \\ \mathbf{V}_{m-\tau} \\ \mathbf{V}_{m+1-\tau} \end{bmatrix} \quad (23)$$

where

$$\mathbf{\Gamma} = \begin{bmatrix} \mathbf{I} & 0 & 0 & 0 & 0 & \cdots & 0 & 0 & 0 & 0 & 0 & 0 \\ \mathbf{P}_{2,1} & \mathbf{P}_{2,2} & 0 & 0 & 0 & \cdots & 0 & 0 & 0 & 0 & 0 & 0 \\ \mathbf{P}_{3,1} & \mathbf{P}_{3,2} & \mathbf{P}_{3,3} & 0 & 0 & \cdots & 0 & 0 & 0 & 0 & 0 & 0 \\ \mathbf{P}_{4,1} & \mathbf{P}_{4,2} & \mathbf{P}_{4,3} & \mathbf{P}_{4,4} & 0 & \cdots & 0 & 0 & 0 & 0 & 0 & 0 \\ \mathbf{F}_1 & \mathbf{F}_2 & \mathbf{F}_3 & \mathbf{F}_4 & \mathbf{F}_5 & \cdots & 0 & 0 & 0 & 0 & 0 & 0 \\ \vdots & \vdots & \vdots & \vdots & \vdots & \ddots & \vdots & \vdots & \vdots & \vdots & \vdots & \vdots \\ 0 & 0 & 0 & 0 & 0 & \cdots & \mathbf{F}_{m-4} & \mathbf{F}_{m-3} & \mathbf{F}_{m-2} & \mathbf{F}_{m-1} & \mathbf{F}_m & 0 \\ 0 & 0 & 0 & 0 & 0 & \cdots & 0 & \mathbf{F}_{m-3} & \mathbf{F}_{m-2} & \mathbf{F}_{m-1} & \mathbf{F}_m & \mathbf{F}_{m+1} \end{bmatrix} \quad (24)$$

$$\mathbf{\Lambda} = \begin{bmatrix} 0 & 0 & 0 & 0 & 0 & \cdots & 0 & 0 & 0 & 0 & 0 & e^{\mathbf{A}t_f} \\ \mathbf{P}_{2,1-\tau} & \mathbf{P}_{2,2-\tau} & 0 & 0 & 0 & \cdots & 0 & 0 & 0 & 0 & 0 & 0 \\ \mathbf{P}_{3,1-\tau} & \mathbf{P}_{3,2-\tau} & \mathbf{P}_{3,3-\tau} & 0 & 0 & \cdots & 0 & 0 & 0 & 0 & 0 & 0 \\ \mathbf{P}_{4,1-\tau} & \mathbf{P}_{4,2-\tau} & \mathbf{P}_{4,3-\tau} & \mathbf{P}_{4,4-\tau} & 0 & \cdots & 0 & 0 & 0 & 0 & 0 & 0 \\ 0 & \mathbf{F}_{2-\tau} & \mathbf{F}_{3-\tau} & \mathbf{F}_{4-\tau} & \mathbf{F}_{5-\tau} & \cdots & 0 & 0 & 0 & 0 & 0 & 0 \\ \vdots & \vdots & \vdots & \vdots & \vdots & \ddots & \vdots & \vdots & \vdots & \vdots & \vdots & \vdots \\ 0 & 0 & 0 & 0 & 0 & \cdots & 0 & \mathbf{F}_{m-3-\tau} & \mathbf{F}_{m-2-\tau} & \mathbf{F}_{m-1-\tau} & \mathbf{F}_{m-\tau} & 0 \\ 0 & 0 & 0 & 0 & 0 & \cdots & 0 & 0 & \mathbf{F}_{m-2-\tau} & \mathbf{F}_{m-1-\tau} & \mathbf{F}_{m-\tau} & \mathbf{F}_{m+1-\tau} \end{bmatrix} \quad (25)$$
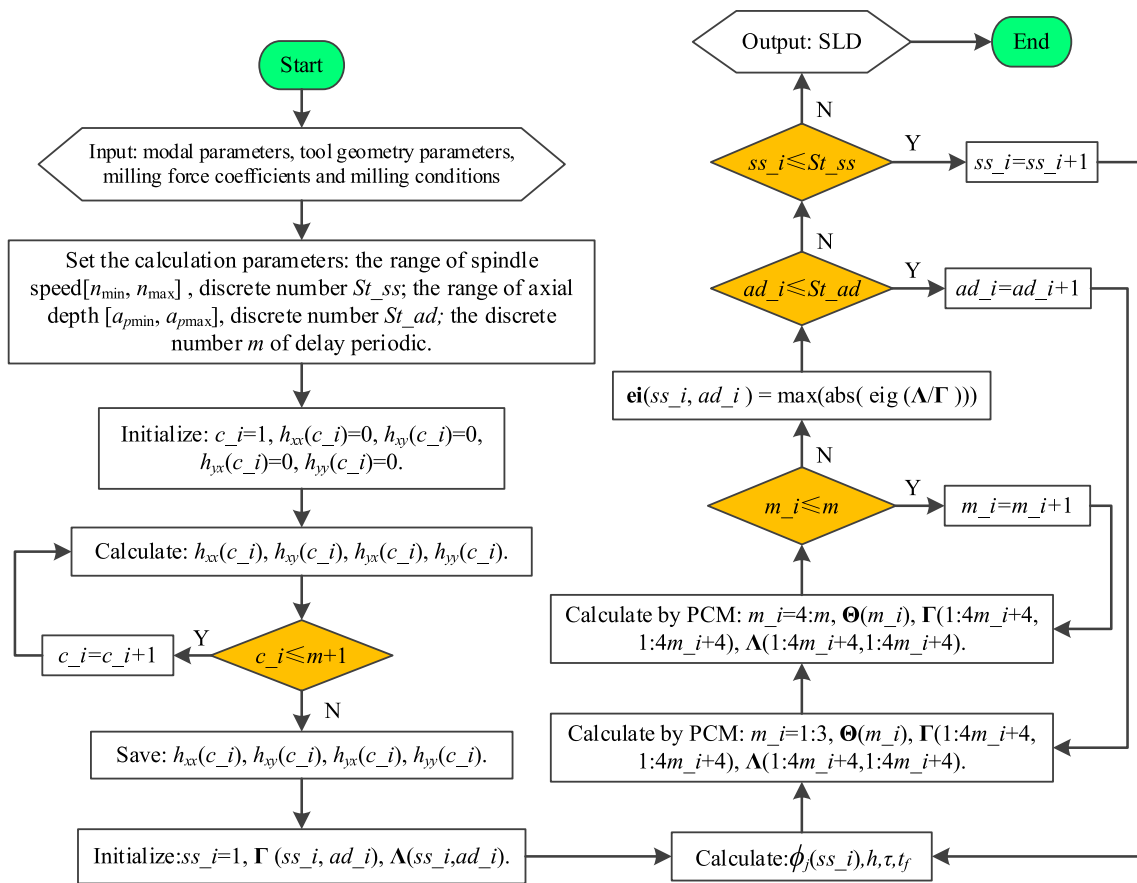
**Fig. 3** Flow chart of obtaining SLD for milling process using MS-PCM

Thus, the state transition matrix in one tooth passing period can be obtained as

$$\mathbf{\Psi} = \mathbf{\Gamma}^{-1}\mathbf{\Lambda} \tag{26}$$

Based on Floquet theory, the judgment criterion of system stability can be proposed according to the spectral radius of the $\mathbf{\Psi}$. If the spectral radius $\rho(\mathbf{\Psi})$ is less than 1, i.e., $\rho(\mathbf{\Psi}) < 1$, the system is in a stable state. If $\rho(\mathbf{\Psi}) > 1$, the system is in an unstable state. But if $\rho(\mathbf{\Psi}) = 1$, the system is in a critically stable state.

In order to clearly understand the obtainment of the SLD, Fig. 3 illustrates the flow of the calculation process.

## 4 Numerical Tests

Here, several typical examples are demonstrated to validate the computational performance of MS-PCM.

### 4.1 Milling System with One-DOF

A one-DOF milling dynamic model is used to verify the effectiveness of the proposed method. Here, the milling tool in the down milling has 2 teeth. The one-DOF model along the feed direction $X$ [12–16] can be expressed as follows

$$m_t\ddot{x}(t) + 2m_t\zeta\omega_n\dot{x}(t) + m_t\omega_n^2 x(t) = -a_p h_{xx}(t)[x(t) - x(t - \tau)] \tag{27}$$

where $\zeta$, $\omega_n$, $m_t$ are the damping ratio, natural angular frequency, and modal mass of the tool system, respectively. $a_p$ is the axial depth of cut.

By substituting $\mathbf{M} = m_t$, $\mathbf{C} = 2m_t\zeta\omega_n$ and $\mathbf{q}(t) = x(t)$ into Eq. (1), Eq. (27) can be further expressed as

$$\dot{\mathbf{V}}(t) = \mathbf{L}\mathbf{V}(t) + \mathbf{\Theta}(t)[\mathbf{V}(t) - \mathbf{V}(t - \tau)] \tag{28}$$

**Table 1** Modal parameters

| $\zeta$ | $\omega_n$ (Hz) | $m_t$ (kg) | $K_t$ (N/m$^2$) | $K_r$ (N/m$^2$) |
|---|---|---|---|---|
| 0.011 | 922 | 0.03993 | $6 \times 10^8$ | $2 \times 10^8$ |

where

$$\mathbf{L} = \begin{bmatrix} -\zeta\omega_n & 1/m_t \\ m_t(\zeta\omega_n)^2 - m_t\omega_n^2 & -\zeta\omega_n \end{bmatrix} \tag{29}$$

$$\mathbf{\Theta}(t) = \begin{bmatrix} 0 & 0 \\ -a_p h_{xx}(t) & 0 \end{bmatrix} \tag{30}$$

Next is to calculate the SLD by using the proposed MS-PCM, 1st SDM and the 2nd FDM. The modal parameters and cutting force coefficients are taken from Ref. [14], as shown in Table 1.

For 1st SDM and 2nd FDM, the Refs. [14, 16] respectively prove that the local truncation error of 1st SDM and 2nd FDM is $O(\tau_3)$. They have 2nd algebraic precision in the mathematical approximation method. However, the local truncation error of MS-PCM is $O(\tau_5)$, that is, it has 4th order algebraic precision. It is known that the MS-PCM has better calculation accuracy over the 1st SDM and 2nd FDM.

In order to intuitively understand the computational performance, a comparison of the convergence rate is carried out for three methods. Firstly, nine groups of milling parameters are given in Table 2.

If $|\mu|$ is the modulus of the maximum eigenvalue of the transition matrix $\mathbf{\Psi}$, $|\mu|$ which is obtained for each group of milling parameters by 1st SDM at $m = 1000$ can be taken as its theoretical value $|\mu_0|$. Because $|\mu|$ is different with different discrete numbers $m$, the absolute value of the difference $\||\mu| - |\mu_0|\|$ between $|\mu|$ and $|\mu_0|$ is defined to measure

the calculation accuracy. Here, $\||\mu| - |\mu_0|\|$ is called the local discrete error. Thus, the variation of the local discrete error with $m$ can be clearly seen according to Fig. 4.

As the discrete number $m$ increases, the local discrete errors $\||\mu| - |\mu_0|\|$ obtained by the three methods gradually approach zero. But at an arbitrary value of $m$ ($m \geq 30$), the MS-PCM has a smaller value of $\||\mu| - |\mu_0|\|$ than the other two methods. In other words, the MS-PCM has a faster convergence rate no matter which $m$ is valued. Therefore, under the same milling parameters, the cave obtained by the MS-PCM is approach to the actual value than the SLD obtained by the other two methods.

A set of SLD curves are compared with each other to further demonstrate the computational performance of the MS-PCM. Here, the radial immersion ratio is selected as 0.05, 0.5 and 1, respectively. Thus, the corresponding SLD curves can be obtained by the 1st SDM, 2nd FDM and MS-PCM for the discrete value $m = 30$ or $m = 60$, as shown in Fig. 5. All calculation procedures are carried out on MATLAB 9.11 installed on a personal computer [Intel(R) Core™ i7-10,700 CPU @ 2.90 GHz 16 GB]. Evidently, the three SLDs are almost identical to each other under the same discrete number and radial immersion ratio, except for slight differences at the peaks of SLDs which will be further analyzed in Sect. 5. However, their computation efficiencies are significantly different as illustrated in Fig. 6. When the computational accuracy is almost equal, the time consumption of MS-PCM is greatly less than 1st SDM and 2nd FDM. If $m = 30$, the time consumption of MS-PCM is about 75% and 50% less than that of the other two methods, respectively. But if $m = 60$, the computational efficiency of MS-PCM is further improved so that its time consumption will be further reduced by 77% and 70%.

In order to reasonably measure the prediction accuracy of the SLD computation method, two statistical formulas are introduced. One is the sum of squared errors (SSE) and another is the arithmetic mean of relative error (AMRE). Their expressions are written as

$$\begin{cases} \text{SSE} = \sum_{i=1}^{r} \left( a_{pi} - a_{pi0} \right)^2 \\ \text{AMRE} = \frac{1}{r} \sum_{i=1}^{r} \frac{|a_{pi} - a_{pi0}|}{a_{pi0}} \end{cases} \tag{31}$$

where $a_{pi}$, $a_{p0}$ are the predicted and expected critical axial depth of cut corresponding to the $i$th spindle speed, respectively. $r$ is the discrete number of the spindle speed.

Now, the SLD corresponding to $a/D = 1$ in Fig. 5 is selected to calculate the SSE and AMRE. According to three SLDs obtained by three methods at $m = 200$, three critical

**Table 2** Simulation parameters for obtaining convergence rate

| No. | Milling parameter | | | $|\mu_0|$ | Stability |
|---|---|---|---|---|---|
| | $a/D$ | $\Omega$/rpm | $a_p$/mm | | |
| 1 | 0.2 | 3000 | 0.7 | 0.9932 | Yes |
| 2 | 0.2 | 3000 | 1.3 | 1.2089 | No |
| 3 | 0.2 | 3000 | 1.9 | 1.3190 | No |
| 4 | 0.5 | 9000 | 0.6 | 0.8920 | Yes |
| 5 | 0.5 | 9000 | 1.2 | 0.9633 | Yes |
| 6 | 0.5 | 9000 | 1.8 | 1.0208 | No |
| 7 | 1.0 | 7000 | 0.9 | 0.9710 | Yes |
| 8 | 1.0 | 7000 | 1.7 | 1.0356 | No |
| 9 | 1.0 | 7000 | 2.5 | 1.0529 | No |

axial depths of cut at the *i*th spindle speed are averaged as the expected critical axial depth of cut $a_{pi0}$. Thus, the prediction accuracy under arbitrary period discrete value can be evaluated for the MS-PCM, 1st SDM and 2nd FDM, as shown in Fig. 7. Obviously, the larger the *m* value, the smaller their SSE and AMRE. But the SSE and AMRE of

the MS-PCM are significantly smaller than the 1st SDM and 2nd FDM at arbitrary *m* value. It can be concluded from Fig. 7b that their AMRE is less than 1% when *m* > 60. In the actual stability analysis, the AMRE is taken as a criterion to reasonably select the period discrete number *m*.
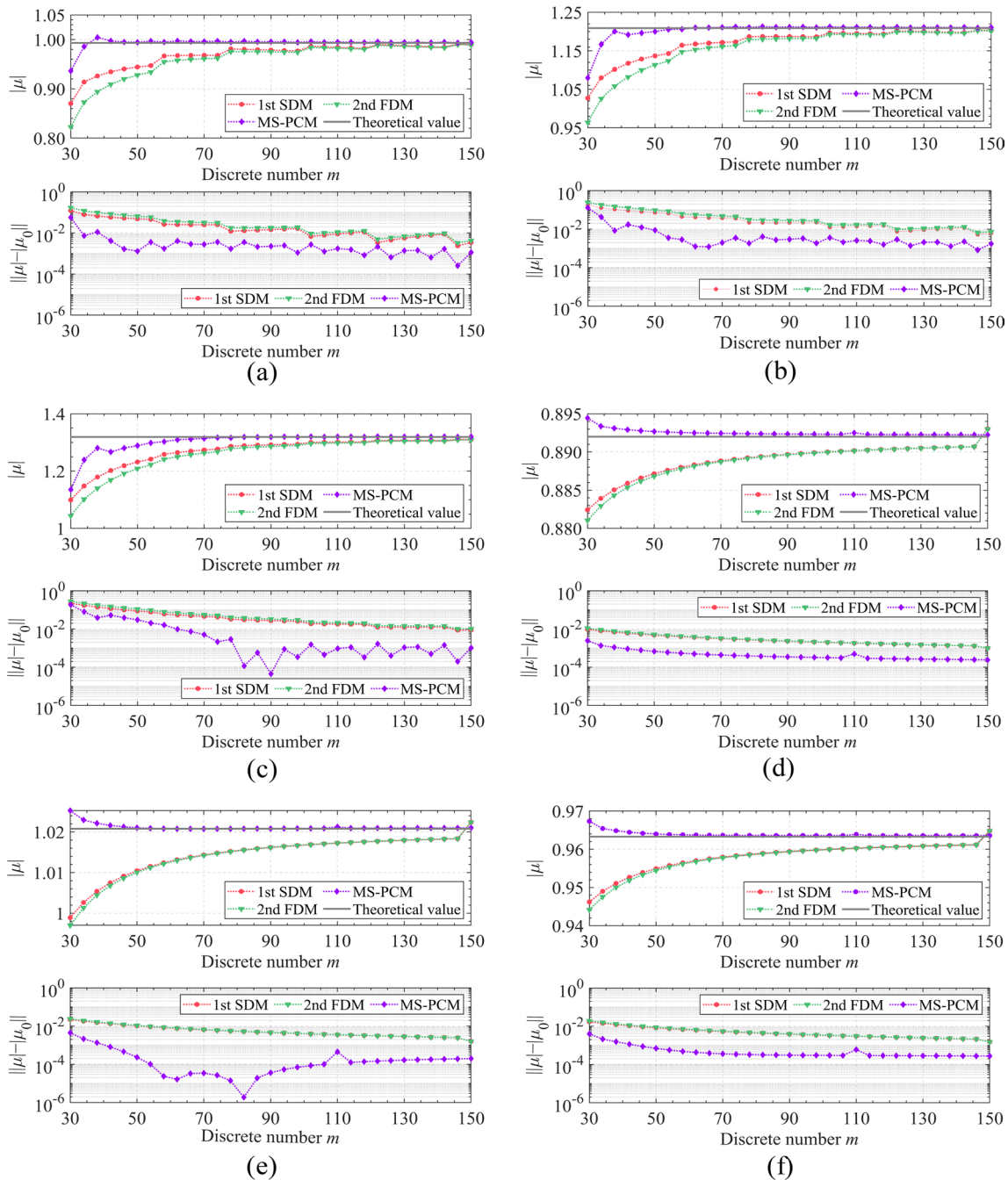


**Fig. 4** Comparisons of convergence rate: **a** $a_p = 0.7$ mm, $\Omega = 3000$ rpm, $a/D = 0.2$; **b** $a_p = 1.3$ mm, $\Omega = 3000$ rpm, $a/D = 0.2$; **c** $a_p = 1.9$ mm, $\Omega = 3000$ rpm, $a/D = 0.2$; **d** $a_p = 0.6$ mm, $\Omega = 9000$ rpm, $a/D = 0.5$; **e** $a_p = 1.2$ mm, $\Omega = 9000$ rpm, $a/D = 0.5$; **f** $a_p = 1.8$ mm, $\Omega = 9000$ rpm, $a/D = 0.5$; **g** $a_p = 0.9$ mm, $\Omega = 7000$ rpm, $a/D = 1.0$; **h** $a_p = 1.7$ mm, $\Omega = 7000$ rpm, $a/D = 1.0$; **i** $a_p = 2.5$ mm, $\Omega = 7000$ rpm, $a/D = 1.0$
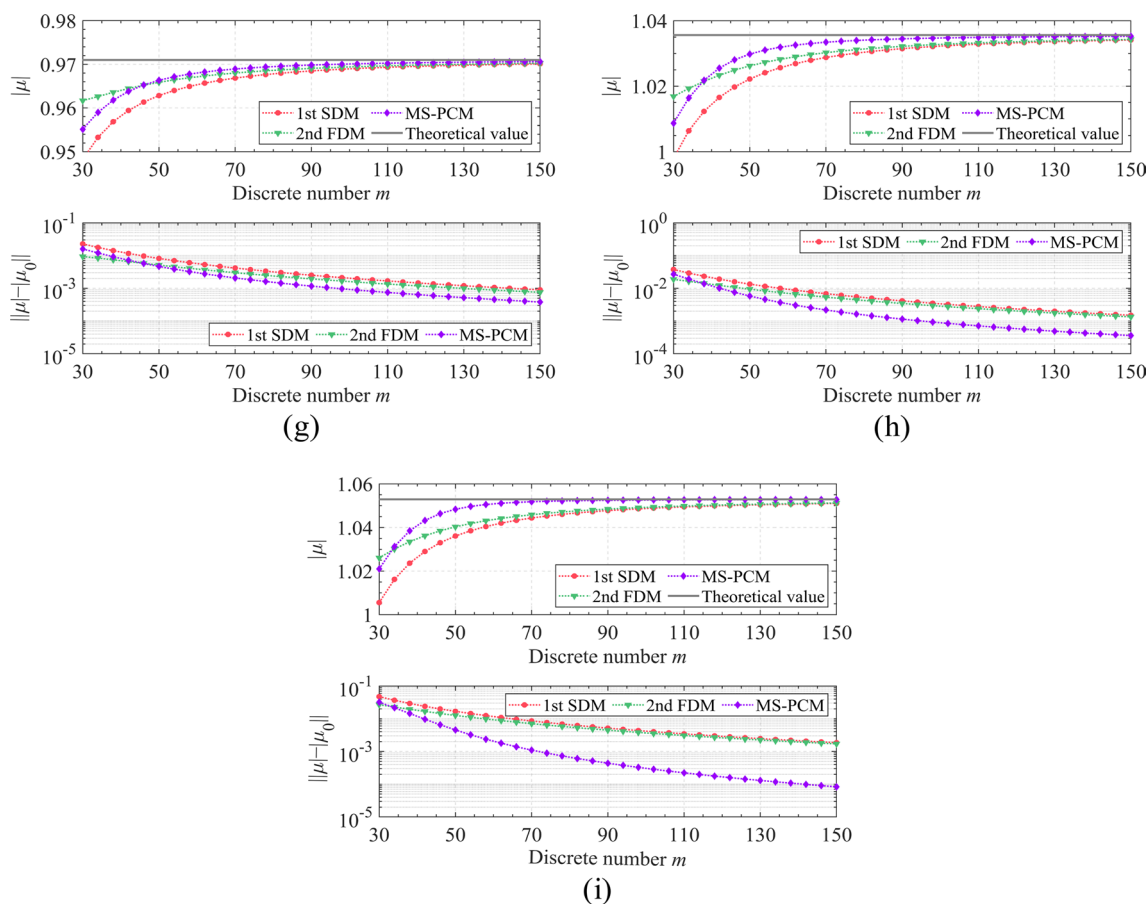
**Fig. 4** (continued)

Figure 8 illustrates the calculation times with the different discrete numbers $m$ for 1st SDM, 2nd FDM and MS-PCM. Obviously, with the increase of discrete number $m$, the computational times of 1st SDM and 2nd FDM are exponential increase approximately whereas the computational time of MS-PCM is linear increase nearly. The main reasons for the different computational efficiency include the following two aspects:

On the one hand, every element in the state transition matrix of 1st SDM relies on the spindle speed and the depth of cut whereas that of the 2nd FDM and the MS-PCM only depend on the spindle speed. If $r_a$ and $r_s$ are respectively the discrete numbers of the spindle speed and the depth of cut, the

1st SDM will calculate $r_a \times r_s \times m$ elements whereas the 2nd FDM and the MS-PCM only need to calculate $r_s$ elements.

On the other hand, the number of state transition matrices of 2nd FDM is related to the discrete number $m$ whereas that of the MS-PCM has nothing to do with the discrete number $m$. Therefore, the 1st SDM and 2nd FDM will calculate $r_a \times r_s \times m$ matrix whereas the MS-PCM only needs to calculate $r_a \times r_s$ state transition matrices.

### 4.2 Milling System with Two-DOF

As shown in Fig. 1, if milling dynamic mode is considered to be two-DOFs, the corresponding DDE [12–16] can be expressed as

$$\begin{bmatrix} m_t & 0 \\ 0 & m_t \end{bmatrix} \begin{bmatrix} \ddot{x}(t) \\ \ddot{y}(t) \end{bmatrix} + \begin{bmatrix} 2m_t\zeta\omega_n & 0 \\ 0 & 2m_t\zeta\omega_n \end{bmatrix} \begin{bmatrix} \dot{x}(t) \\ \dot{y}(t) \end{bmatrix} + \begin{bmatrix} m_t\omega_n^2 & 0 \\ 0 & m_t\omega_n^2 \end{bmatrix} \begin{bmatrix} x(t) \\ y(t) \end{bmatrix}$$
$$= a_p \begin{bmatrix} -h_{xx}(t) & -h_{xy}(t) \\ -h_{yx}(t) & -h_{yy}(t) \end{bmatrix} \left\{ \begin{bmatrix} x(t) \\ y(t) \end{bmatrix} - \begin{bmatrix} x(t-\tau) \\ y(t-\tau) \end{bmatrix} \right\}$$

(32)

**Fig. 5** Comparisons of SLDs predicted by three methods of one-DOF with different discretization numbers *m*. **a** and **b** *a/D* = 0.05; **c** and **d** *a/D* = 0.5; **e** and **f** *a/D* = 1
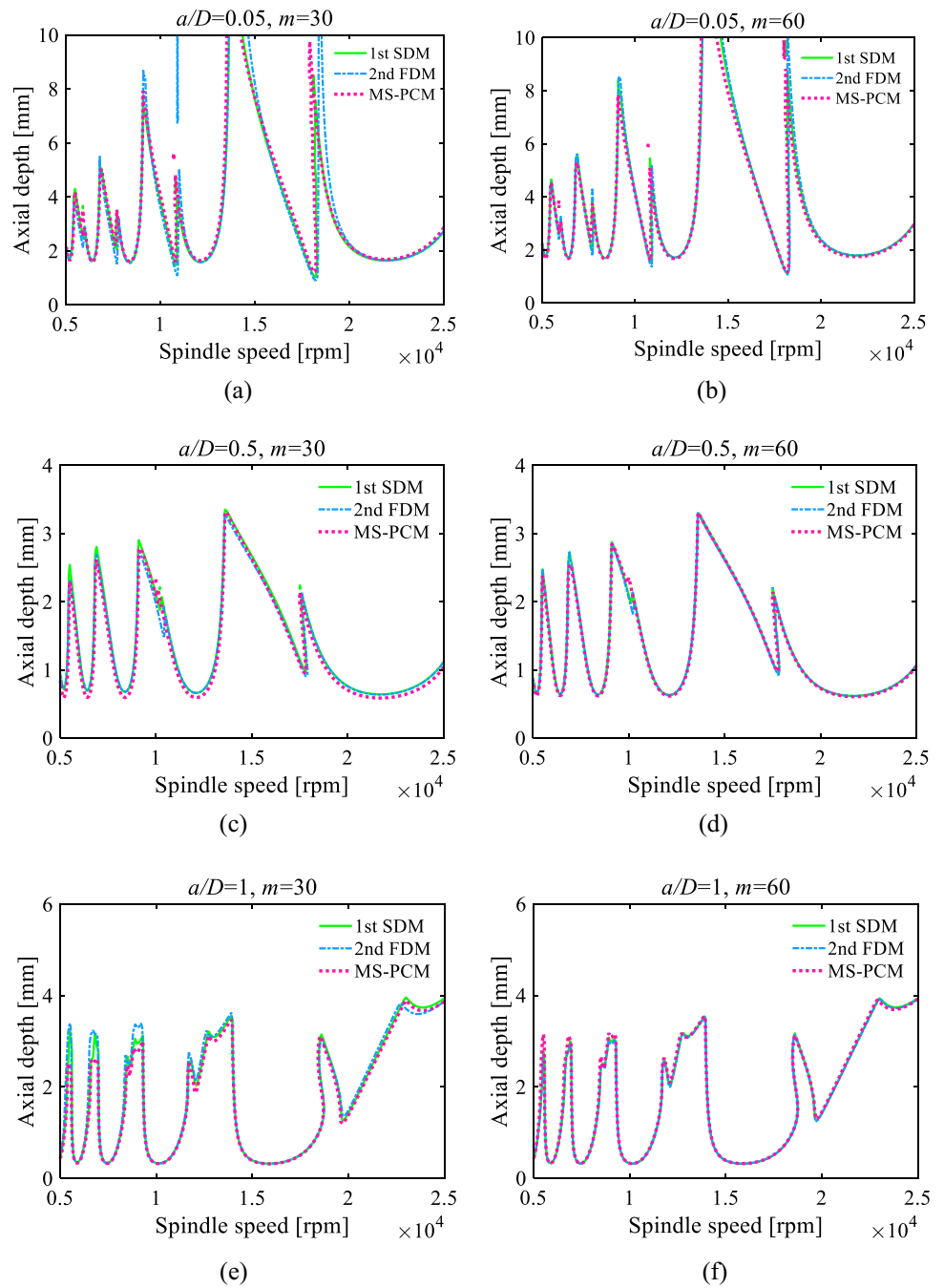


Let $\mathbf{M} = \begin{bmatrix} m_t & 0 \\ 0 & m_t \end{bmatrix}$, $\mathbf{C} = \begin{bmatrix} 2m_t\zeta\omega_n & 0 \\ 0 & 2m_t\zeta\omega_n \end{bmatrix}$, $\mathbf{q}(t) = \begin{bmatrix} x(t) \\ y(t) \end{bmatrix}$, $\mathbf{p}(t) = \mathbf{M}\dot{\mathbf{q}}(t) + \mathbf{C}\mathbf{q}(t)/2$, and $\mathbf{V}(t) = [\mathbf{q}(t)\ \mathbf{p}(t)]^{\mathrm{T}}$, Eq. (32) can be further described as

$$\dot{\mathbf{V}}(t) = \mathbf{L}\mathbf{V}(t) + \mathbf{\Theta}(t)[\mathbf{V}(t) - \mathbf{V}(t - \tau)] \tag{33}$$

where

$$\mathbf{L} = \begin{bmatrix} -\zeta\omega_n & 0 & 1/m_t & 0 \\ 0 & -\zeta\omega_n & 0 & 1/m_t \\ (\zeta^2 - 1)\omega_n^2 m_t & 0 & -\zeta\omega_n & 0 \\ 0 & (\zeta^2 - 1)\omega_n^2 m_t & 0 & -\zeta\omega_n \end{bmatrix} \tag{34}$$
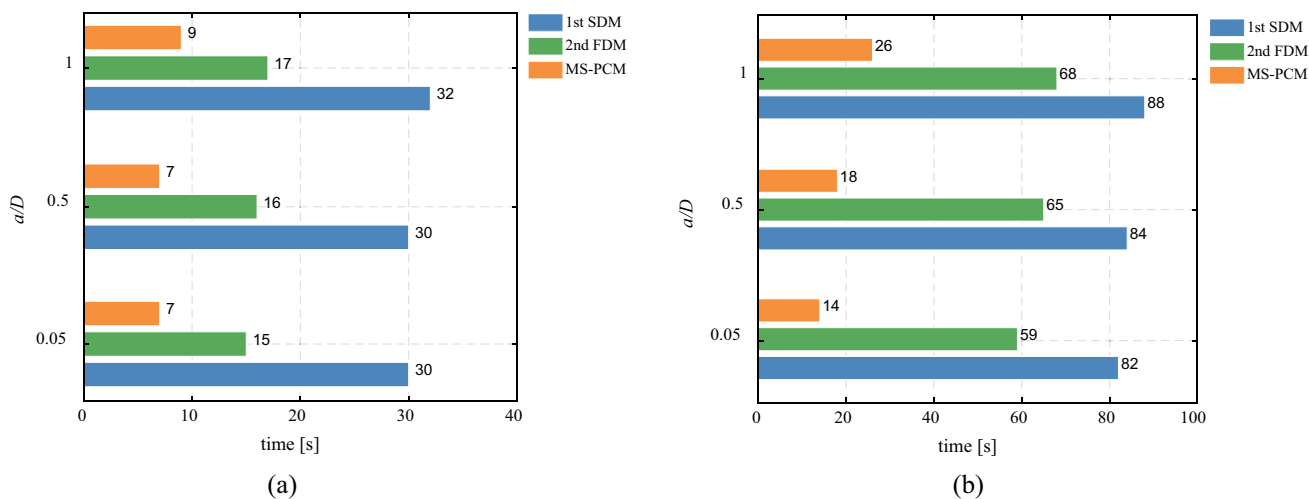
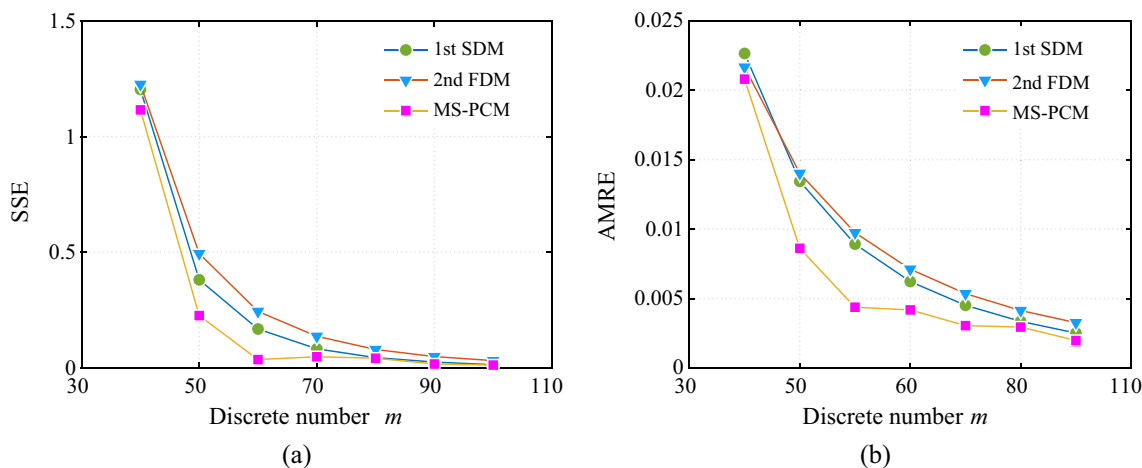**Fig. 6** Comparison of computing time. **a** $m = 30$; **b** $m = 60$



**Fig. 7** Comparisons of SSE and AMRE. **a** SSE; **b** AMRE

$$\Theta(t) = \begin{bmatrix} 0 & 0 & 0 & 0 \\ 0 & 0 & 0 & 0 \\ -a_p h_{xx}(t) & -a_p h_{xy}(t) & 0 & 0 \\ -a_p h_{yx}(t) & -a_p h_{yy}(t) & 0 & 0 \end{bmatrix} \tag{35}$$

in which the meaning of each parameter is the same as Sect. 4.1.

Because the MS-PCM has faster computing efficiency and higher computing precision, the SLD curve calculated by the MS-PCM at m = 200 can be completely thought to be a theoretical SLD. Here, three special cutting conditions are selected to analyze the stability of down milling. They are the minimal radial immersion ratio of $a/D = 0.05$, the

maximum radial immersion ratio of $a/D = 1$ and the half-tooth radial immersion ratio of $a/D = 0.5$, respectively.

When the $m$ is 40, the SLDs of the two-DOFs milling system can be obtained under the condition of 200 intervals of spindle speed $\Omega$ and 100 intervals of axial depth of cut $a$, as shown in Table 3. When $a/D = 0.05$ and $a/D = 0.5$, the SLDs obtained by the MS-PCM almost completely coincided with the theoretical SLD. However, there are still subtle differences among these two SLDs obtained by the 1st SDM and 2nd FDM and the theoretical SLD. But when $a/D = 1$, three SLD curves are coincident with the theoretical curve. Therefore, the MS-PCM has an advantage in computational accuracy over the 1st SDM and 2nd FDM.
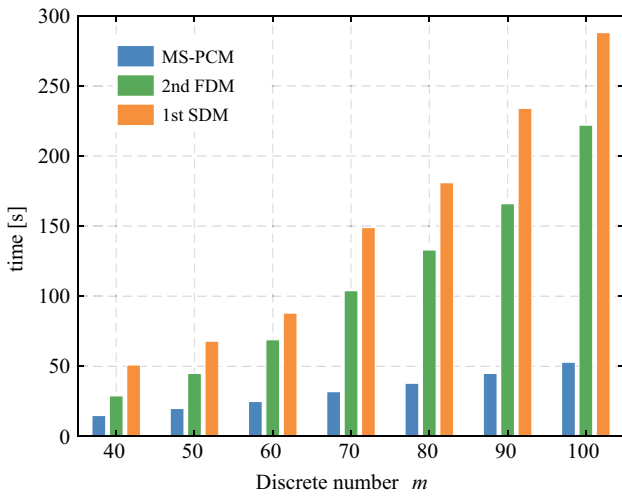
**Fig. 8** Comparisons of simulation time

## 5 Simulation and Experimental Verification

It is known from Sect. 4.1 that the SLD curves obtained by the three methods are basically the same at $m = 30$. However, there are still significant differences at the peaks of SLD curves. The actual prediction effect of MS-PCM at the peaks can be validated according to the cutting force and vibration displacement. The specific details of the simulation on cutting force and vibration displacement can be found in Ref. [5]. Here, one peak in Fig. 5e is taken as an example in which the spindle speed ranges from 22,000 to 24,000 rpm whereas the axial depth of cut is 3.3–4.1 mm. Thus, near the specified peak, 29 groups of parameter combinations of the spindle speed with the axial depth of cut can be selected to analyze their stability, as shown in Fig. 9.
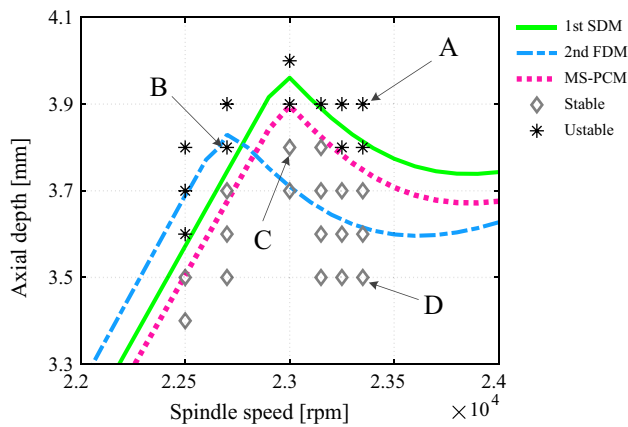
**Table 3** SLDs of two-DOF milling system

**Fig. 9** Prediction accuracy verification of local SLD boundaries, $a/D = 1$ and $m = 30$

The simulation method can be used to obtain the corresponding cutting force and vibration displacement of these 29 groups of parameter combinations. According to the time-domain waveform, it can be judged whether the cutting process is stable under the specific parameter combination. "*" means the simulation result is unstable, and "◇" is stable. From the simulation results of 29 groups of parameter combinations, it can be seen that MS-PCM can more accurately predict the stability boundary than 1st SDM and 2nd FDM. Figure 10 shows the simulation results of the four groups of typical parameters corresponding from A to D in Fig. 9. It is worth noting that the red symbol "○" is the sampling of vibration displacement when the milling tool rotates one circle. Obviously in stable cutting conditions, whether the waveform and peak value of cutting force or those of vibration displacement cannot almost change. Moreover, the periodic sampling value of vibration displacement is basically on the same horizontal line. Under the condition of unstable cutting, the waveform and peak value of cutting force have very obvious irregular changes as well as those of vibration displacement. In addition, the periodic sampling value of vibration displacement is not in one horizontal line, but in one irregular curve.

A set of milling experiments are adopted to validate the actual prediction results of the proposed method. All of the experiments are done on a three-axis CNC machine tool XKA715, as shown in Fig. 11. The workpiece material is aluminum alloy 7075-T7451. The milling tool is a three-tooth flat end mill with a diameter of $D = 12$ mm. The radial depth of cut is 0.24 mm so the radial immersion ratio is $a/D = 0.2$. The cutting force coefficients are $K_t = 13.85 \times 108$ N/m$^2$ and $K_r = 11.65 \times 108$ N/m$^2$, respectively. The modal parameters of the tool are listed in Table 4.

The SLD calculated by MS-PCM ($m = 100$) is shown in Fig. 12a. 9 groups of parameter combinations are selected near the SLD curve for milling experiments. The cutting force signal and the surface morphology of the workpiece machined surface can be used to comprehensively judge the stability of the milling process. The stability results of 9 groups of parameter combinations are shown in Table 5 and Fig. 12a. "*" represents being unstable whereas "◇" stable. Figure 12b gives the time-domain diagram and frequency spectrum diagram of the measured milling forces corresponding to A and B, as well as the surface morphology of the machined workpiece. It can show the milling process is stable at B with the spindle speed of 5750 rpm and the axial depth of cut of 0.75 mm. In this case, the frequency domain signal of milling force only contains the integral multiple of tooth passing frequency whose expression is TF = $\Omega N/60$. But if the parameter combination of A (5700 rpm, 1.0 mm) is selected to machine a workpiece, the frequency domain signal of milling force contains other so-called non-tooth passing frequencies in addition to the integral multiple of tooth passing frequency. In fact, these non-tooth passing frequencies belong to the chatter frequencies. Therefore, the milling process of A is unstable. As has further been analyzed above, the proposed MS-PCM is accurate and effective to predict milling stability.

# 6 Conclusion

A linear multi-step predictor–corrector method is adopted for milling stability prediction in this paper. Based on the DDE of the dynamic milling process, the Milne formula and the Simpson formula as the predictor- and the corrector-term are used to constructing the state transition matrix. According to the Floquet theory, the stability lobe can be obtained.

The analysis of the error convergence rate and computational efficiency is done to validate the MS-PCM by using a one-DOF milling model. The results show that whether the computational accuracy or the computational time, the MS-PCM has advantages. The bigger the discrete number $m$ is, the more obvious the advantage of MS-PCM is in computational efficiency.

The simulation results on the cutting force and vibration displacement of 29 groups of parameter combinations show that the proposed method has higher prediction accuracy. Again, 9 groups of parameter combinations are further determined to carry out the milling experiments. Whether the frequency domain signal of milling force or the surface morphology of the machined workpiece can demonstrate the proposed method is effective and accurate in the actual prediction of the milling stability.

**Fig. 10** Signal simulation of vibration and force. **a** and **b** point A; **c** and **d** point B; **e** and **f** point C; **g** and **h** point D
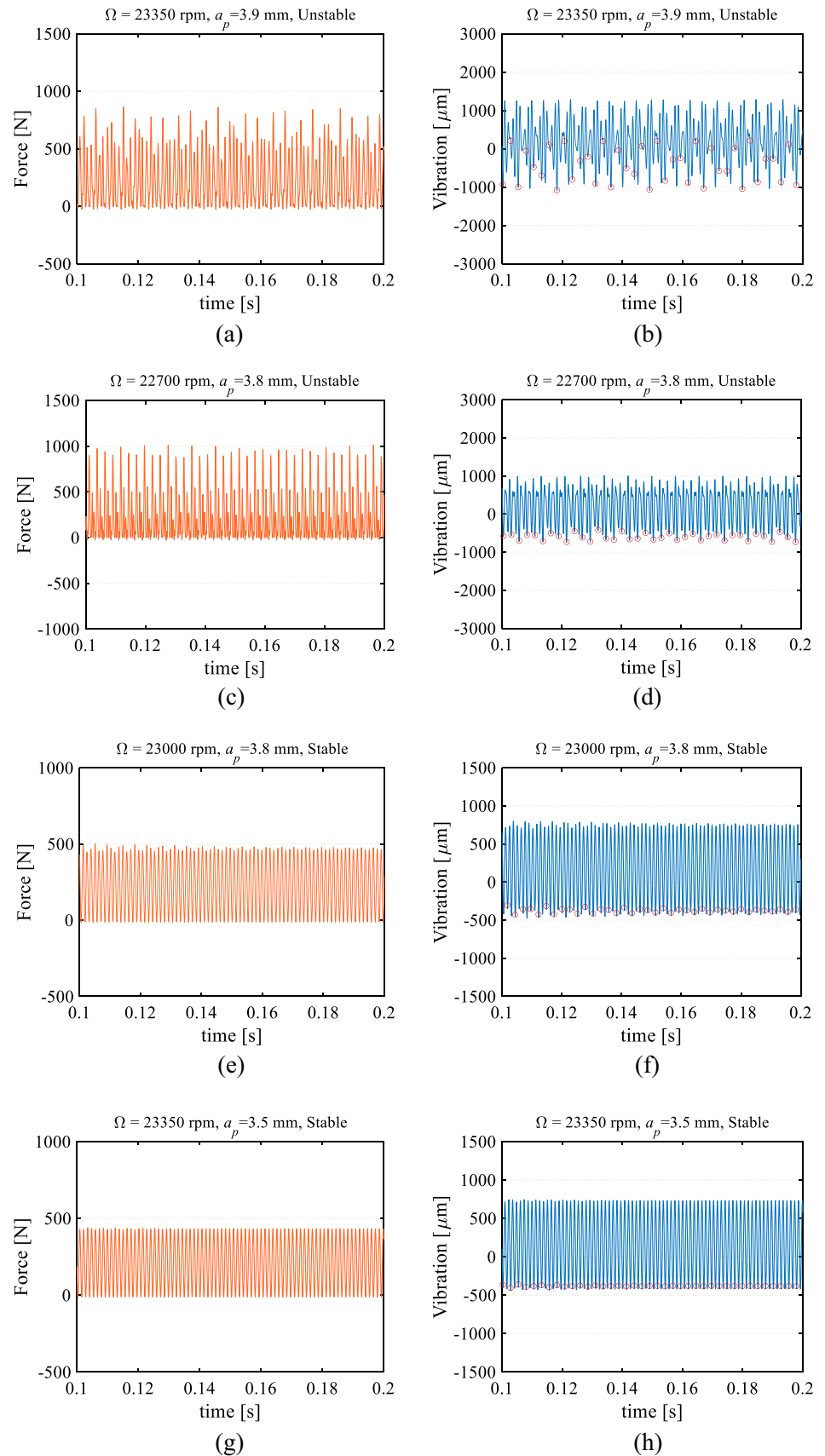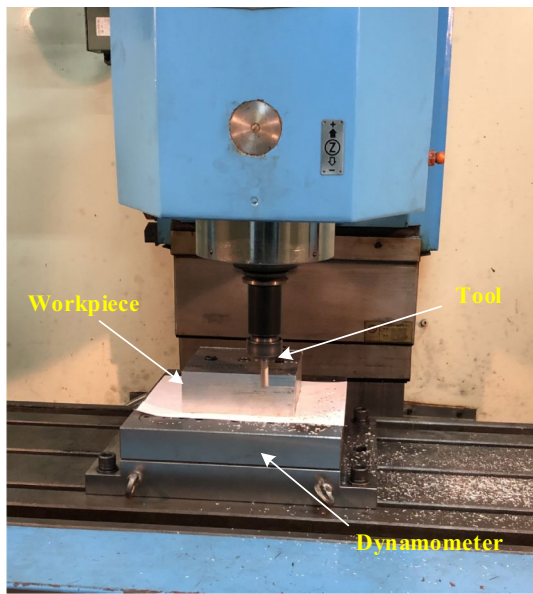
**Fig. 11** Experimental setup

**Table 4** Modal parameters of tool

| $\zeta$ | $\omega_n$ (Hz) | $m_t$ (kg) | $k$ ($\times 10^6$ N/m) |
|---|---|---|---|
| 0.011 | 922 | 0.03993 | 2.31 |

**Table 5** Cutting parameters and stability

| No. | Parameter combination | | Stability |
|---|---|---|---|
| | $\Omega$ (rpm) | $a_p$ (mm) | |
| 1 | 4050 | 0.75 | Yes |
| 2 | 4130 | 0.6 | No |
| 3 | 4600 | 0.7 | Yes |
| 4 | 4820 | 0.7 | No |
| 5 | 5300 | 0.4 | No |
| 6 | 5350 | 0.65 | Yes |
| 7 | 5500 | 0.5 | No |
| 8 | 5700 | 1.0 | Yes |
| 9 | 5750 | 0.75 | No |

## Appendix 1: Integral Equation

Integral equations are equations involving integral operations on unknown functions, as opposed to differential equations. Many mathematical physics problems need to be solved by integral equations or differential equations.

The most basic form of an integral equation is Fredholm integral equation of the first kind:
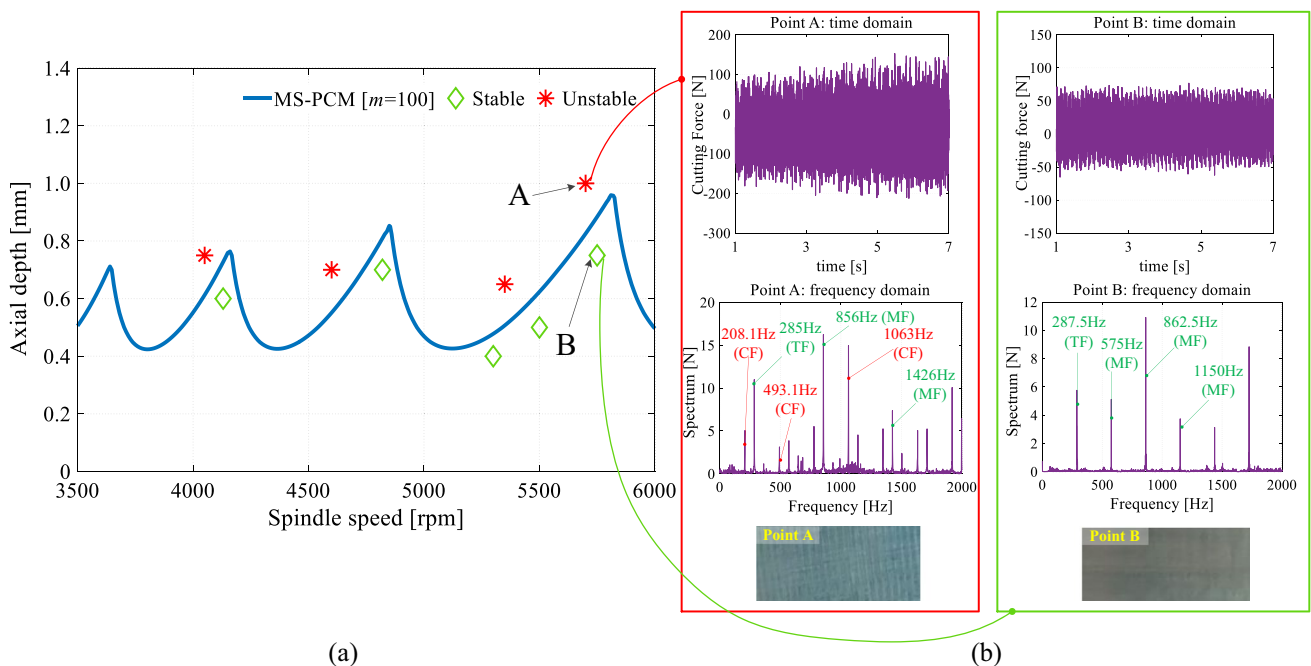
$$f(x) = \int_a^b K(x,t)\phi(t)dt,$$



(a)

(b)

**Fig. 12** Experimental verification of the stability prediction boundary obtained by applying the proposed method. **a** Stability lobe diagram and selection of cutting parameters; **b** Cutting force in time and frequency domains and workpiece surface topography after processing

where, $f$ and $K$ are known, $K$ is also called the kernel function, and $\phi$ is the unknown function to be sought. The upper and lower limits of integration $a$, $b$ are constants.

If the unknown function appears both inside and outside the integral sign, the equation is called a Fredholm integral equation of the second kind:

$$\phi(x) = f(x) + \lambda \int_a^b K(x,t)\phi(t)dt,$$

as an unknown factor, $\lambda$ plays a role similar to the eigenvalue in linear algebra.

If the upper or lower bound of the integration is a variable, the equation is called the Volterra integral equation. The Volterra integral equations of the first and second kind have the following forms:

$$f(x) = \int_a^x K(x,t)\phi(t)dt,$$

$$\phi(x) = f(x) + \lambda \int_a^x K(x,t)\phi(t)dt,$$

All the above equations are called homogeneous if $f$ is always 0, otherwise, they are called inhomogeneous.

## Appendix 2: Linear Multi-step Methods

1. Fourth-order Milne formula:

$$y_{n+4} = \frac{4}{3}h\left[2f_{n+3} - f_{n+2} + 2f_{n+1}\right],$$

where $y' = f(x,y)$, its local truncation error is:

$$R_{n+4} = \frac{14}{45}h^5 y^{(5)}(x_n) + O(h^6).$$

2. Fourth-order Simpson formula:

$$y_{n+2} = \frac{h}{3}\left[f_{n+2} + 4f_{n+1} + f_n\right],$$

where $y' = f(x,y)$, its local truncation error is:

$$R_{n+4} = \frac{1}{90}h^5 y^{(5)}(x_n) + O(h^6).$$

## Appendix 3: Partial Formula Expression

$\mathbf{G}_{i+1} = 8/9h^2 e^{3h\mathbf{L}}\mathbf{\Theta}_{i+1}\mathbf{\Theta}_{i+4}$; $\mathbf{G}_{i+2} = \left(1/3\mathbf{I} - 4/9h\mathbf{\Theta}_{i+4}\right)he^{2h\mathbf{L}}\mathbf{\Theta}_{i+2}$;

$\mathbf{G}_{i+3} = \left(4/3\mathbf{I} + 8/9h\mathbf{\Theta}_{i+4}\right)he^{h\mathbf{L}}\mathbf{\Theta}_{i+3}$.

$\mathbf{F}_{i+1-\tau} = \mathbf{G}_{i+1}$; $\mathbf{F}_{i+2-\tau} = \mathbf{G}_{i+2}$; $\mathbf{F}_{i+3-\tau} = \mathbf{G}_{i+3}$;

$\mathbf{F}_{i+4-\tau} = 1/3h\mathbf{\Theta}_{i+4}$; $\mathbf{F}_i = 1/3h\mathbf{\Theta}_{i+4}e^{4h\mathbf{L}}$;

$\mathbf{F}_{i+1} = \mathbf{G}_{i+1}$; $\mathbf{F}_{i+2} = e^{2h\mathbf{L}} + \mathbf{G}_{i+2}$;

$\mathbf{F}_{i+3} = \mathbf{G}_{i+3}$; $\mathbf{F}_{i+4} = -\mathbf{I}$.

$\mathbf{P}_{2,1} = -\left(e^{h\mathbf{L}} + 1/2he^{h\mathbf{L}}\mathbf{\Theta}_1\right)$; $\mathbf{P}_{2,2} = \left(\mathbf{I} - 1/2h\mathbf{\Theta}_2\right)$;

$\mathbf{P}_{2,1-\tau} = -1/2e^{h\mathbf{L}}\mathbf{\Theta}_1$; $\mathbf{P}_{2,2-\tau} = -1/2h\mathbf{\Theta}_2$;

$\mathbf{P}_{3,1} = -\left(e^{2h\mathbf{L}} + 1/3he^{2h\mathbf{L}}\mathbf{\Theta}_1\right)$; $\mathbf{P}_{3,2} = -4/3he^{h\mathbf{L}}\mathbf{\Theta}_2$;

$\mathbf{P}_{3,3} = \left(\mathbf{I} - 1/3\mathbf{\Theta}_3\right)$; $\mathbf{P}_{3,1-\tau} = -1/3he^{2h\mathbf{L}}\mathbf{\Theta}_1$;

$\mathbf{P}_{3,2-\tau} = -4/3he^{h\mathbf{L}}\mathbf{\Theta}_2$; $\mathbf{P}_{3,3-\tau} = -1/3h\mathbf{\Theta}_3$.

$\mathbf{P}_{4,1} = -\left(e^{3h\mathbf{L}} + 3/8he^{3h\mathbf{L}}\mathbf{\Theta}_1\right)$; $\mathbf{P}_{4,2} = -9/8he^{2h\mathbf{L}}\mathbf{\Theta}_2$;

$\mathbf{P}_{4,3} = -9/8he^{h\mathbf{L}}\mathbf{\Theta}_3$;

$\mathbf{P}_{4,4} = -\left(\mathbf{I} + 3/8h\mathbf{\Theta}_4\right)$; $\mathbf{P}_{4,1-\tau} = -3/8he^{3h\mathbf{L}}\mathbf{\Theta}_1$;

$\mathbf{P}_{4,2-\tau} = -9/8he^{2h\mathbf{L}}\mathbf{\Theta}_2$;

$\mathbf{P}_{4,3-\tau} = -9/8he^{h\mathbf{L}}\mathbf{\Theta}_3$; $\mathbf{P}_{4,4-\tau} = -3/8h\mathbf{\Theta}_4$.

## Declarations

**Conflict of interest** The authors declare that they have no conflict of interest.

## References

1. Altintas, Y., & Weck, M. (2004). Chatter stability of metal cutting and grinding. *CIRP Annals-Manufacturing Technology, 53*(2), 619–642.
2. Quintana, G., & Ciurana, J. (2011). Chatter in machining processes: A review. *International Journal of Machine Tools and Manufacture, 51*(5), 363–376.
3. Altintas, Y. (2012). *Manufacturing automation: Metal cutting mechanics, machine tool vibrations, and CNC design*. Cambridge University Press.
4. Faassen, R. P. H., Van de Wouw, N., Oosterling, J. A. J., et al. (2003). Prediction of regenerative chatter by modelling and analysis of high-speed milling. *International Journal of Machine Tools and Manufacture, 43*(14), 1437–1446.
5. Schmitz, T. L., & Smith, K. S. (2019). *Machining dynamics: Frequency response to improved productivity*. Springer International Publishing.
6. Altintas, Y., Stepan, G., Merdol, D., et al. (2008). Chatter stability of milling in frequency and discrete time domain. *CIRP Journal of Manufacturing Science and Technology, 1*(1), 35–44.
7. Balachandran, B. (2001). Nonlinear dynamics of milling processes. *Philosophical Transactions of the Royal Society of London. Series A: Mathematical, Physical and Engineering Sciences, 359*(1781), 793–819.

8. Wiercigroch, M., & Budak, E. (2001). Sources of nonlinearities, chatter generation and suppression in metal cutting. *Philosophical Transactions of the Royal Society of London. Series A: Mathematical, Physical and Engineering Sciences, 359*(1781), 663–693.

9. Altintas, Y., & Budak, E. (1995). Analytical prediction of stability lobes in milling. *CIRP Annals-Manufacturing Technology, 44*(1), 357–362.

10. Merdol, S., & Altintas, Y. (2004). Multi-frequency solution of chatter stability for low immersion milling. *ASME-Journal of Manufacturing Science and Engineering, 126*(3), 459–466.

11. Bayly, P. V., Halley, J. E., Mann, B. P., et al. (2003). Stability of interrupted cutting by temporal finite element analysis. *ASME Journal of Manufacturing Science and Engineering, 125*, 220–225.

12. Insperger, T., & Stepan, G. (2002). Semi-discretization method for delayed systems. *International Journal for numerical methods in engineering, 55*(5), 503–518.

13. Insperger, T., & Stepan, G. (2004). Updated semi-discretization method for periodic delay-differential equations with discrete delay. *International Journal for Numerical Methods in Engineering, 61*, 117–141.

14. Insperger, T., Stepan, G., & Turi, J. (2008). On the higher-order semi-discretizations for periodic delayed systems. *Journal of Sound and Vibration, 313*(1), 334–341.

15. Ding, Y., Zhu, L. M., Zhang, X. J., et al. (2010). A full-discretization method for prediction of milling stability. *International Journal of Machine Tools and Manufacture, 50*(5), 502–509.

16. Ding, Y., Zhu, L. M., Zhang, X. J., et al. (2010). Second-order full-discretization method for milling stability prediction. *International Journal of Machine Tools and Manufacture, 50*(10), 926–932.

17. Quo, Q., Sun, Y. W., & Jiang, Y. (2012). On the accurate calculation of milling stability limits using third-order full-discretization method. *International Journal of Machine Tools and Manufacture, 62*(1), 61–66.

18. Liu, Y. L., Zhang, D. H., & Wu, B. H. (2012). An efficient full-discretization method for prediction of milling stability. *International Journal of Machine Tools and Manufacture, 63*, 44–48.

19. Sun, Y., & Xiong, Z. (2017). High-order full-discretization method using Lagrange interpolation for stability analysis of turning processes with stiffness variation. *Journal of Sound and Vibration, 386*, 50–64.

20. Ozoegwu, C. G., & Omenyi, S. N. (2016). Third-order least squares modelling of milling state term for improved computation of stability boundaries. *Production & Manufacturing Research, 4*(1), 46–64.

21. Ozoegwu, C. G., Omenyi, S. N., & Ofochebe, S. M. (2015). Hyper-third order full-discretization methods in milling stability prediction. *International Journal of Machine Tools and Manufacture, 92*, 1–9.

22. Tang, X., Peng, F., Yan, R., et al. (2017). Accurate and efficient prediction of milling stability with updated full-discretization method. *The International Journal of Advanced Manufacturing Technology, 88*(9–12), 2357–2368.

23. Yan, Z., Wang, X., Liu, Z., et al. (2017). Third-order updated full-discretization method for milling stability prediction. *The International Journal of Advanced Manufacturing Technology, 92*(5), 2299–2309.

24. Niu, J. B., Ding, Y., Zhu, L. M., et al. (2014). Runge–Kutta methods for a semi-analytical prediction of milling stability. *Nonlinear Dynamics, 76*(1), 289–304.

25. Li, M. Z., Zhang, G. J., & Huang, Y. (2013). Complete discretization scheme for milling stability prediction. *Nonlinear Dynamics, 71*(1–2), 187–199.

26. Zhang, Z., Li, H. G., & Meng, G. (2015). A novel approach for the prediction of the milling stability based on the Simpson method. *International Journal of Machine Tools and Manufacture, 99*, 43–47.

27. Li, Z., Yang, Z., Peng, Y., et al. (2016). Prediction of chatter stability for milling process using Runge–Kutta-based complete discretization method. *The International Journal of Advanced Manufacturing Technology, 86*(1), 943–952.

28. Mostaghimi, H., Park, S. S., Lee D. Y., et al. (2023). Prediction of tool tip dynamics through machine learning and inverse receptance coupling. *International Journal of Precision Engineering and Manufacturing*. Advance online publication. https://doi.org/10.1007/s12541-023-00831-6

29. Kang, G., Kim, J., Choi, Y., et al. (2022). In-process identification of the cutting force coefficients in milling based on a virtual machining model. *International Journal of Precision Engineering and Manufacturing, 23*(8), 839–851.

30. Qin, C., Tao, J., & Liu, C. (2019). A novel stability prediction method for milling operations using the holistic-interpolation scheme. *Proceedings of the Institution of Mechanical Engineers, Part C: Journal of Mechanical Engineering Science, 233*(13), 4463–4475.

31. Dai, Y., Li, H., Xing, X., et al. (2018). Prediction of chatter stability for milling process using precise integration method. *Precision Engineering, 52*, 152–157.

32. Lou, W. D., Qin, G. H., & Zuo, D. W. (2021). Investigation on cotes-formula-based prediction method and its experimental verification of milling stability. *Journal of Manufacturing Processes, 64*, 1077–1088.

33. Wu, Y., You, Y., Liu, A., et al. (2021). A correction method for milling stability analysis based on local truncation error. *The International Journal of Advanced Manufacturing Technology, 115*, 2873–2887.

34. Wu, Y., You, Y., Liu, A., et al. (2020). An implicit exponentially fitted method for chatter stability prediction of milling processes. *The International Journal of Advanced Manufacturing Technology, 106*(5), 2189–2204.

35. Liu, K., Zhang, Y., Gao, X., et al. (2021). Improved semi-discretization method based on predictor-corrector scheme for milling stability analysis. *The International Journal of Advanced Manufacturing Technology, 114*(11), 3377–3389.

36. Qin, G. H., Lou, W. D., Wang, H. M., et al. (2022). High efficiency and precision approach to milling stability prediction based on predictor-corrector linear multi-step method. *The International Journal of Advanced Manufacturing Technology, 122*(3–4), 1933–1955.

37. Wei, X., Miao, E., & Ye, H. (2022). Analytical prediction of three dimensional chatter stability considering multiple parameters in milling. *International Journal of Precision Engineering and Manufacturing, 23*(7), 711–720.

38. Chen, D., Zhang, X. J., & Ding, H. (2020). Generalized numerical differentiation method for stability calculation of periodic delayed differential equation: Application for variable pitch cutter in milling. *International Journal of Precision Engineering and Manufacturing, 21*, 2027–2039.

39. Stoer, J., & Bulirsch, R. (2013). *Introduction to numerical analysis*. Springer Science & Business Media.

40. Mann, B. P., Young, K. A., Schmitz, T. L., et al. (2005). Simultaneous stability and surface location error predictions in milling. *ASME Journal of Manufacturing Science and Engineering, 127*(3), 446–453.
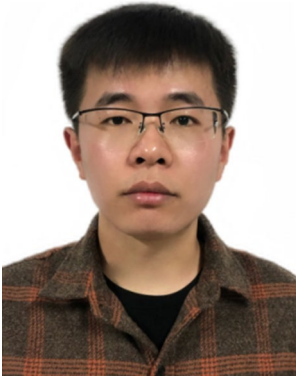
**Weida Lou** was born in Shandong, China, in 1994. He received the B.S. and M.S. degree in School of Aeronautics Manufacturing Engineering from Nanchang Hangkong University, Nanchang, China, in 2017 and 2020 respectively. He is currently working toward the Ph.D. degree of Aeronautics and Astronautics Manufacturing Engineering at Northwestern Polytechnical University, Xi'an, China. His research interests include dynamic modeling and simulation of machining process and stability analysis of cutting system.
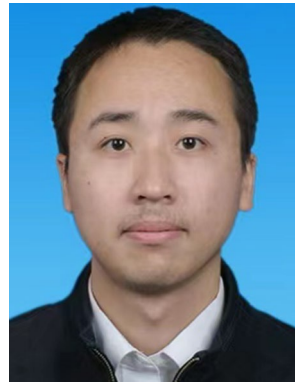


**Xiaochun Lai** received the M.S. degree in Signal and Information Systems from Nanchang Hangkong University, Nanchang, China, in 2007. She is currently an associate professor and her research interests include Signal and information processing, tool wear analysis and detection.



**Guohua Qin** was born in Jiangxi, China, in 1970. He holds a Ph.D. in Aeronautical and Astronautical Manufacturing Engineering from Northwestern Polytechnical University, Xi'an, China, in 2005. He is currently a professor in School of Aeronautics Manufacturing Engineering, Nanchang Hangkong University, Nanchang, China. His research interests include analysis and optimization of workpiece fixturing, mathematical analysis and deformation control of machining process, prediction and inverse of residual stress in aeronautical monolithic components, and Fault diagnosis and health management.



**Yuanjun Hou** received the Ph.D. degree in Mechanical Manufacturing and Automation from Nanjing University of Aeronautics and Astronautics, Nanjing, China, in 2020. He is currently a lecturer in School of Aeronautics Manufacturing Engineering, Nanchang Hangkong University, Nanchang, China. His research interests include intelligent precision manufacturing and advanced manufacturing technology.